Best Practices for Solar Irradiance Measurements with Rotating Shadowband Irradiometers

v 2.0

October 19th, 2023

S. Wilbert, N. Geuder,
M. Schwandt, B. Kraas,
W. Jessen, R. Meyer,
B. Nouri, A. Forstinger,
F. Vignola

Contents

1. Introduction

Large-scale solar plant projects require rigorous solar resource assessments. The main solar resource task is to determine the incident solar radiation on the collector. Before the plant construction satellite radiation data is used in combination with ground data to accurately estimate inter-annual variability and long-term mean values. Hence, reliable ground measurements have to be collected for sound analysis of solar plant projects. Unfortunately, high accuracy irradiance data are scarcely available in many regions which are attractive for solar energy applications, in particular if it comes to direct or diffuse irradiance. The accurate monitoring of solar energy systems requires measurements of the solar radiation that is used by the collectors. For bifacial PV systems the diffuse horizontal irradiance (DHI) is of interest to determine the rear-side irradiance and for concentrating collectors the direct normal irradiance (DNI) is required. Rotating Shadowband Irradiometers (RSIs) are one option to determine the global horizontal irradiance (GHI), DHI and DNI.

To obtain ground measurements of the quality to monitor solar energy systems or to augment and validate satellite-derived irradiance data, general guidelines should be followed regarding site selection and preparation, instrument selection, maintenance procedures, and data quality monitoring. Best practices for radiation measurements for solar energy with various available instrument options are included in the "Best Practices Handbook for the Collection and Use of Solar Resource Data for Solar Energy Applications" [Sengupta2021]. If RSIs are used, specific recommendations as those presented in this document are of interest.

Appropriate irradiance sensors for ground measurements should be selected based on the required accuracy of the measurements, maintenance and power available at the site for the duration of the measurement period, and environmental factors such as soiling rates. For example, radiometers and in particular pyrheliometers can be severely affected by soiling [Pape2009]. Pyrheliometers also require expensive and complex support devices such as automatic solar trackers. Thus, the uncertainty of resource assessment depends heavily on a regular maintenance routine, at least a few times a week for pyrheliometers, and data quality suffers if this maintenance routine cannot be sustained. RSI's advantages compared to thermopile sensors when operated under the measurement conditions of remote weather stations are their lower soiling susceptibility, ease of installation and operation, low power demand, and comparatively lower cost. RSIs are also known as RSP (Rotating Shadowband Pyranometers) or RSR™ (Rotating Shadowband Radiometers). Here we use the notation RSI to refer to either instrument measuring irradiance by use of a rotating shadowband. The initially lower accuracy of RSIs, that can yield uncertainties of 5 to 10 % or more, is notably improved with proper calibration of the sensors and corrections of the systematic deviations associated with use of a Si-photodiode based sensor. Main causes of the systematic deviations are the limited spectral sensitivity and, to a lesser extent, the temperature dependence of the Si-photodiode commonly used in most RSIs.

Besides the systematic deviations of the sensor response, a significant contribution to the measurement uncertainty originates from the sensor calibration at the manufacturer, where systematic biases are not removed. For proper calibration however, the proposed adjustments need to be considered in the calibration procedure. While well documented standards exist for the calibration of pyrheliometers and pyranometers ([ISO9059 1990], [ISO9846 1993], [ISO9847 2023]), their application for RSIs is not obvious and no specific standards exist for RSIs.

This document contains RSI-specific best practices for the following tasks:

- Requirements on the selection of a site for a measurement station
- Installation, operation and maintenance of a measurement station, including the case of remote sites
- Documentation and quality control of the measurements
- Correction of systematic errors
- Calibration protocol for RSIs

The uncertainty of RSI measurements is also briefly described.

2. General description of continuously rotating RSIs

A continuously rotating RSI itself consists of a horizontally mounted LI-COR pyranometer in combination with a shadowband. The shadowband is mounted below the sensor in an angle of (approximately) 45° and typically rotates once or twice per minute around the sensor (see Figure 1). During rotation, the shadowband casts a shadow on the sensor, blocking out the sun for a short moment. Some RSIs have shadowbands that may rotate several times per minute during rapidly changing irradiance conditions.

The irradiance value measured over time during the rotation results in a typical measurement curve, which is called burst or sweep (see Figure 2). The chronological course of the signal is shown over the "measurement point number" (instead of time), the point density depending on the sampling frequency of each device.

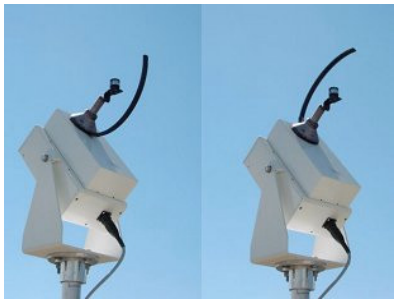

Figure 1: One example for an RSI: Rotating Shadowband Pyranometer (RSP) in normal position (left) and during rotation (right).

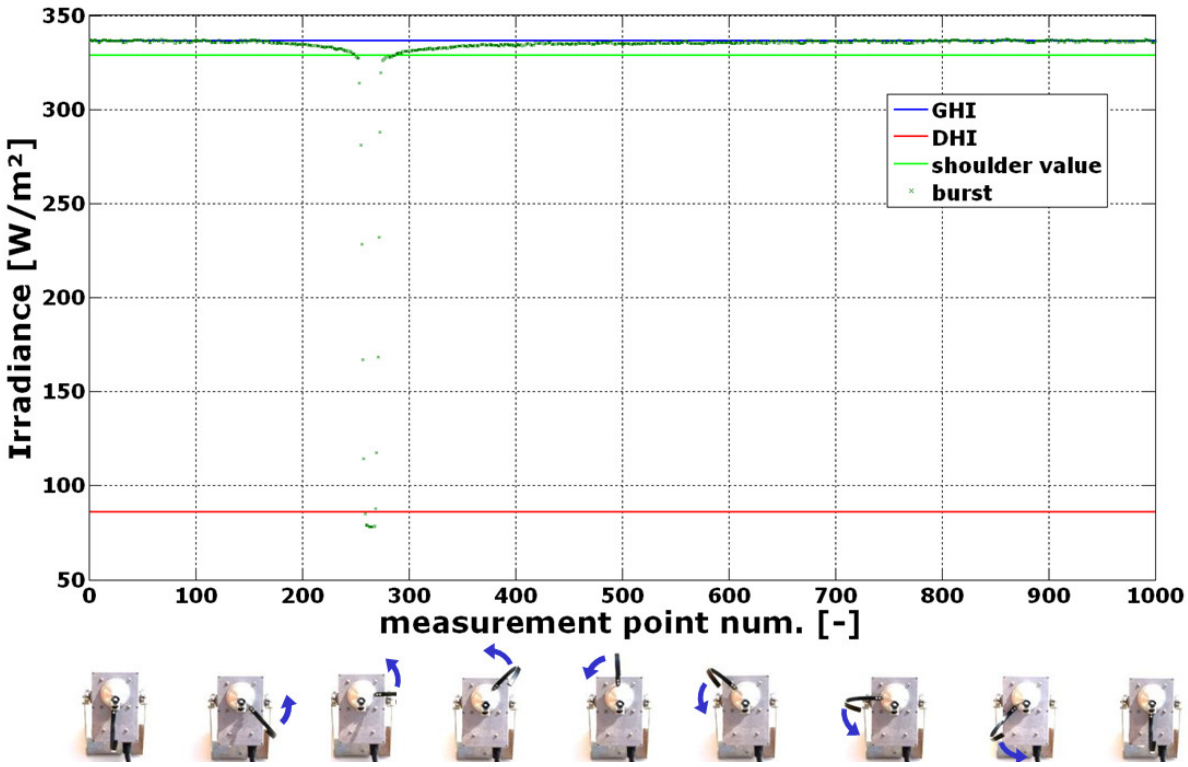

Figure 2: Burst (sweep) with sensor signal and the derived GHI, shoulder values and the DHI.

At the beginning of the rotation, the pyranometer measures global horizontal irradiance (GHI). In the moment when the center of the shadow falls on the center of the sensor it basically only detects diffuse horizontal irradiance (DHI). However, the shadowband covers some portion of the sky so that the minimum of the burst is less than the DHI. Thus, shoulder values are determined and the difference between the average of the shoulder values and the GHI is added to the minimum of the curve to obtain the DHI. Subsequently, direct normal irradiance (DNI) is calculated by the datalogger using GHI, DHI and the solar elevation angle computed from the datalogger time and coordinates of the location.

One version of such an algorithm defines the distance (in measurement points) between the positions of the minimum (p_{min}) and the maximum of the burst's slope as the well width (w_{well}). The position of the left shoulder value $p_{shoulder,L}$ is then defined as half the well width left of p_{min}:

$$p_{shoulder,L} = p_{min} - w_{well}/2.$$

The right shoulder value is found correspondingly. The shoulder value is the average of the left and the right shoulder value. The difference between the GHI and the shoulder value is added to the minimum of the curve to obtain the DHI. Finally, DNI is calculated using GHI, DHI and the solar elevation angle.

DHI and DNI are only determined approximately once or a few times per minute, but GHI measurements can be sampled in a higher frequency without the rotation of the

shadowband, e.g. every second. The variation of the GHI also contains some information about the change of DNI. Different algorithms are used to determine the minutely average of DHI and DNI from the burst and the more frequent GHI measurement. These algorithms are presented below in the descriptions of different existing RSI systems that are summarized in the next subsection.

Note that the name "continuously rotating RSI" refers to the fact that the rotation that occurs for the measurement of a burst is continuous. Between the rotations the shadowband stays in the rest position as mentioned above. Other RSIs do not measure the full burst, but only a few points of the burst and subsequently rotate the shadowband to the positions corresponding to the shoulder values and the minimum of the burst. These RSIs are not described in this report in detail.

The LI-COR pyranometer is a practically instantaneously measuring device, but shows dependence on temperature and also lacks uniform spectral response in its sensitive range between 0.4 and 1.2 µm. As the whole range of incoming radiation lies mainly between 0.25 and over 2.5 µm and its spectrum is varying with changing atmospheric conditions, this results in systematic errors in the measurements based on the spectral distribution of the incident radiation. Some major changes in spectral distribution can be detected at low solar elevations when a significant part of the near infrared solar radiation (outside the pyranometer's sensitive range) is absorbed by water vapor and thus changes not detectable by the sensor. Calibration of the LI-COR pyranometers is carried out by the manufacturer against an Eppley Precision Spectral Pyranometer for 3 to 4 days under daylight conditions [LI-COR2001]. Depending on the exact sky conditions during that period, a certain bias of the determined calibration constant might occur. This bias results both from the bias in the irradiance measurements from the Eppley PSP and the changing spectral distribution. The additional calibration of the RSIs is important and corresponding methods are described later.

The most important specifications of the commonly used pyranometer are listed in Table 1. For many years the LI-200SA pyranometer was used in RSIs with continuous rotation. Since 2015 the slightly updated LI-200R pyranometer is available which has very similar specifications, but a much shorter response time.

Main causes of the systematic deviations are the limited spectral sensitivity and temperature dependence of the SI-photodiode commonly used in most RSIs. The corresponding correction functions have to be considered an essential part of the measurement instrument and are described later.

2.1. Existing RSI instruments

Below are three examples of commercially used RSI instruments with continuous rotation. Please note, that the complete required system consists of the RSI instrument itself, a datalogger or control unit, that controls the instrument (rotation) and also evaluates the collected bursts. The control unit might also apply the important correction functions for reducing systematic errors. Specifications and distributors

contact details are listed in Table 2, Table 3 and Table 4. RSIs with discontinuous rotation are not described here due to their different principle of operation.

Table 1: Specifications of the used LICOR LI-200SA and LI-200R pyranometers.

	LI-COR
Response time (95 %)	10 µs (LI-200SA), <1 µs (LI-200R)
Zero off-set (T_{amb}-drift by 5 K/h)	—
Non-stability	< ±2 %/a
Non-linearity (<3000 W/m²)	±1 %
Temperature response (-10...+40°C)	±0.15 %/K
Directional response	< ±5 %
Calibration error (manufacturer calibration)	±3 (LI-200R), ±5 % (LI-200SA)
Viewing angle	2π sr

Table 2: CSPS Twin-RSI by CSP Services GmbH

Instrument name:	CSPS Twin-RSI
Manufacturer:	CSP Services GmbH
Contact:	info@cspservices.de
Homepage:	www.cspservices.de
Pyranometer type:	Two LI-COR LI-200 pyranometers (R; only old models with SA version)
Sensor temperature measurement:	Yes
Datalogger:	Campbell Scientific CR series (CR800/ CR1000 / CR1000x / ...)
Solar position algorithm:	Astronomical Almanac's Algorithm from [Michalsky1988]
sampling rate GHI:	1 / second
Rotation frequency:	1 / 30 seconds (alternating bursts are measured for the two pyranometers)
Method to derive DHI and DNI 1min averages from the measurement during the rotation:	DHI: calculated after rotation every minute for each pyranometer, averaged every minute from two samples (current value and value from last minute) DNI: calculated every second by 1 second GHI samples from the same pyranometer and 1 minute DHI average, averaged to 1 minute resolution Averages of the pairs of irradiances from both pyranometers used to obtain final DHI, DNI and GHI
Further remarks:	- set-up with two separately calibrated pyranometers for redundancy, high accuracy and reliability - rotation speed controlled shadowband additionally enables measurement of circumsolar irradiance [Wilbert2018]

Table 3: RSR by Irradiance, Inc.

Instrument name:	RSR2, RSR3
Manufacturer:	Irradiance, Inc.
Contact:	info@irradiance.com
Homepage:	irradiance.com
Pyranometer type:	LI-COR LI-200 (SA for RSR2, R for RSR3)
Sensor temperature measurement:	No (ambient only, plus correction)
Datalogger:	Campbell Scientific CR1000, CR800
Solar position algorithm:	Campbell Scientific built-in (Michalsky)
sampling rate GHI:	1 / (5 seconds)
Rotation frequency:	At least 1 / (30 seconds), at most 1 / (5 seconds) if 20 W/m² change in GHI
Method to derive DHI and DNI 1min averages from the measurement during the rotation:	Averaged after calculation of DHI/DNI for each rotation
Further remarks:	None

Table 4: RSP by Reichert GmbH

Instrument name:	RSP 4G (also previous versions 3G, 2G exist)
Manufacturer:	Reichert GmbH
Contact:	reichert@reichertgmbh.de
Homepage:	wilmers.com, suntrace.de, cspservices.de
Pyranometer type:	LI-COR LI-200 (R or SA)
Sensor temperature measurement:	Yes
Datalogger:	Campbell Scientific CR800/CR1000
Solar position algorithm:	Campbell Scientific built-in (Michalsky)
sampling rate GHI:	1 / second
Rotation frequency:	1 / (60 seconds)
Method to derive DHI and DNI 1min averages from the measurement during the rotation:	DHI: calculated after rotation every minute, averaged every minute from two samples (current value and value from last minute) DNI: calculated every second by 1 second GHI sample and DHI determined from two 1 minute samples of DHI, then averaged to 1min resolution
Further remarks:	none

3. Measurement site selection

Selection of a good site that is representative of the surrounding environment is critical in order to obtain valuable and accurate meteorological measurement data. In general, the site should be representative of the meteorological conditions in the area of interest and should not be affected by obstructions like close hills, buildings, structures, or trees that might not affect the entire solar installation. Guidelines for site selection are contained separately for each measurement variable in the WMO Guide to Instruments and Measurements [WMO2018]. Further guidelines are also available in the "Best Practices Handbook for the Collection and Use of Solar Resource Data for Solar Energy Applications." [Sengupta2021], section 3.5, which is prepared by IEA PVPS task 16. The guidelines are summarized and completed with a few practical recommendations in the following section.

3.1. General requirements

- Dimensions for the selected measurement site should be at least 10×10 m², with a recommended area free of obstructions of 25×25 m²
- A horizontal surface is desirable. Sloped surfaces should be avoided in particular if not characteristic for the planned or existing solar installation.
- Accessibility by motor vehicle should be given in order to facilitate installation and O&M activities, while public access should be restricted or avoided. Preferably, a protection fence should be constructed around the site provided that it does not interfere with the sensor's normal operation. Rooftop installations are also acceptable as long as there is safe and easy access to the roof.
- Remote data transmission should be possible (e.g., via mobile phone network, ethernet or other). Operators should check the communication options before final site selection. For mobile phone networks, check signal strength and integrity. Where no other communication means are available, satellite data transfer might also be considered.
- Avoid power lines crossing the site, either underground or above ground. Other than to minimize the influence of shadows, this is for safety reasons in order to avoid electric shocks in case of touching the power lines, while it is also important to eliminate the influence of electric fields from alternating current power lines that might disturb the measurements by inducing noise signals in the cabling of the station. Contact local utilities for the location of buried utility lines.

3.2. Additional requirements for the measurement of solar radiation

- Any obstruction above the horizon affects the measurements and can drastically reduce the measured irradiance. On sites where it is not possible to avoid obstructions, the complete details of the horizon and any obstructions should be included in the description of the station to facilitate a subsequent assess-

ment of their impact. The horizon profile that also affects the planned or existing solar installation does not have to be avoided, but should be documented. Refer to the Best Practices Handbook for more details.

- As large solar installations will not be affected in great parts by smaller obstacles, such as single trees or buildings, a sufficient distance should be kept. The distance between radiation sensors and such obstacles should be at least 10 times the difference in height between the sensor and the obstacle.
- No bright artificial light or reflections from reflective surfaces that can increase the radiation measurement should inflict the sensor.
- Avoid construction features that may attract roosting or nesting birds, otherwise the use of spike strips or other measures is recommended. Hollow tubes or openings in cabinets should be capped to avoid bees and other insects from nesting at/in the station.

3.3. Additional requirements for co-located measurement of wind

- Wind towers should be set up in an azimuthal direction from the solar sensors that minimizes shadows during the entire year (i.e., to the north in the northern hemisphere and to the south in the southern hemisphere). Even guy cables of the towers should never shade the radiometers.

3.4. Locations that should be avoided

The operator is finally responsible for the selection of an adequate location for installing measurement stations. Even as the conditions of each prospective site are particular, some general recommendations on locations that should be avoided can be established (list is not extensive).

- Depressions where water might accumulate after rainfall or floods
- Erosion-prone areas
- Steep slopes
- Sheltered hollows
- Existing high vegetation or places with fast growing seasonal vegetation
- Shaded areas
- Swamps
- Areas with snow drifts
- Dry and dusty areas with a frequented road close by
- Irrigated agricultural land
- Large industrial areas
- Proximity to emitting sources of dust, aerosols, soot or other particles

If the location of the planned or existing solar installation is also affected by these issues, it might be acceptable or even recommendable to measure under these adverse conditions. E.g. if a roof top PV installation is planned in the center of a large industrial area, the solar measurement station should also be installed at this site. If a solar park is planned close to, but outside the industrial area, it is not recommendable to measure inside the industrial area. The same example can be made with steep slopes, dusty areas, particle emissions or shaded areas, too. In any case, the effects of these adverse conditions have to be considered when comparing the data with other data sets such as satellite or weather model derived radiation.

3.5. Security and surveillance

To avoid theft or damage of equipment, the station should be properly monitored and protected by at least surrounding it by a fence as described below. In solar power plants the security measures for the power plant itself should be sufficient. For stations installed on roofs the access to the roof should be limited to authorized personnel.

- Fences should be of sufficient height to avoid or discourage people and animals climbing over.
- The irradiance sensor must be installed at a higher level than the fence height.
- It is recommended to secure a location within private property or property of public institutions.
- For security and surveillance reasons it is recommended to have local staff near the station that can control the station at regular intervals and can report possible vandalism, lightning damage, malfunction, etc. These intervals should be determined based on O&M needs, accessibility, funding, and other factors.

4. Measurement station hardware and installation

4.1. Power supply

For unattended remote sites, automatic weather stations must provide their own power source through a PV installation with backup battery of proper capacity. The PV module and backup battery must be specified to supply at least the amount of energy needed by the system to ensure proper operation during the time that the maintenance team requires detecting and correcting the power supply failure, which should normally not exceed one week.

If the system does not provide its own power source, but relies on an electrical grid connection it should be equipped with an UPS (uninterruptable power supply). The UPS should send an alarm when it starts providing backup power, so that the operation and maintenance personnel can react within the duration time of the battery.

4.2. Grounding and shielding

The equipment should be properly grounded to prevent lightning damage, and also shielded to prevent e.g. radio frequency interferences. Proper connection strategy is important to prevent ground loops that can affect the measurements.

4.3. Communications, data transfer and storage

Automated data transfer should be used in order to have access to the measurement system continuously or in daily scale. Modems connected to the mobile network with at least GPRS connection are an appropriate solution for most remote stations. Alternatively, ethernet, radio-frequency connectivity, wired modem with internet access or WIFI can be used if corresponding facilities are available. Satellite communication could be an option (e.g. Iridium) in very remote areas. If the data are downloaded manually, very frequent site visits are required in order to avoid any data loss due to data storage restrictions or malfunctions, and also for quick detection of measurement error and instrument malfunction. Therefore, automated data transfer should be used.

4.4. Environmental conditions

Instruments, meteorological measurement stations and support structures must be able to withstand tough atmospheric and environmental conditions, requiring the lowest possible maintenance effort. Lightning damage protection, e.g. a grounding rod, should be foreseen. The equipment should be specified at least for the expected temperature range (e.g. -30°C to +55°C) and wind gusts, depending on the climate on site. All parts accessible from outside should be safe against bite damage by animals and made of stainless material to prevent corrosion. Cables and other equipment must be UV resistant. All mechanical parts and joints of the meteorological station must be capable to withstand wind, thermal, earthquake, and other natural stresses that should be identified before system deployment. Opportunities for bird and insect nesting within components should be minimized if possible.

4.5. Documentation of site and installation

The following documentation should be included with the measurement equipment:

- Layout diagram for the whole station area (within the fence)
- Drawings of required foundations, grounding poles and all other necessary civil works on the measurement site
- Installation and operation manuals for each device or sensor
- Listing of installed sensors with sensor specification, serial number, calibration protocol and history
- General station layout description and wiring diagram
- Maintenance instructions for high-quality data acquisition and transmission
- At the site of the meteorological station it is necessary to indicate basic emergency procedures and operator contact data to facilitate local staff reporting of any anomalous situation.
- Photographical documentation of the station, the instruments and station surroundings including 360º panorama photo from the position of the irradiance instrument after completing the installation of the station with free view of the station surroundings, from North over East to North (or alternatively 8 single photos towards: NN, NE, EE, SE, SS, SW, WW, NW)
- Optionally, web cams can be installed at the site in order to allow for visual inspection of the station

5. Operation and maintenance

Regular maintenance of the equipment of a meteorological station assures its proper functioning, reduces the effects of possible malfunctions through early detection, and avoids or reduces the number and duration of data gaps.

5.1. General requirements

Maintenance personnel and personnel performing continuous data quality control should maintain a gap-free, transparent documentation of sensor cleaning events and all notable events such as sensor realignment, strong observed sensor soiling, malfunctions and their correction. This documentation is preferably saved in electronic databases, associated with the data with exact timestamp and information which measurement parameter(s) is/are affected. Detailed information recorded (see documentation list below) can be of the highest value if data quality issues arise. Any abnormal events, the condition of the instruments, infrastructure and environment should be documented on any occasion when such observations have been made. Pictures with date/time stamps are useful for this purpose and provide a valuable visible insight on the condition of the instruments. The documentation should be shared with the personnel responsible for the data control at least every month.

Instrument maintenance and operation should only be performed by qualified, trained personnel. The frequency and extent of maintenance visits also depends on the instrumentation and site characteristics, and the planning stage of the measurement campaign should include maintenance consideration. The cost of maintenance during a long-term measurement campaign can easily exceed the initial cost of the instrumentation. The planned cost of operation and maintenance has to be considered in the budgetary framework, and additional provisions should be made to handle any unexpected malfunction.

5.2. Prevention from power outages

In case of grid power supply, the equipment should be protected from power outage by providing an uninterruptable power supply (UPS) as mentioned in section 4.1, which also needs regular check-up. Since the efficiency of UPS batteries tends to degrade over time and under severe environmental conditions, they must be tested at regular intervals (e.g., every 6 months or even shorter intervals) and replaced if necessary.

5.3. Instrument cleanliness

RSI instruments are not as prone to soiling effects as other radiation sensors such as pyrheliometers [Pape2009]. Nevertheless, they require regular cleaning. The cleaning interval is site-specific and should be validated at the beginning of the measurement period by analyzing the immediate change in irradiance values when the instrument is cleaned. The cleaning interval should be adjusted in a way that soiling effects never cause more than a 1-2 % degradation in measurements. Each cleaning and the state of the sensors should be documented (e.g. by data flagging techniques)

and the measurement values should be checked to evaluate the effect of cleaning on the recorded values. Taking photographic records of the sensor with time/date stamps before and after the cleaning events is recommended if soiling is visible or if the cleaning frequency is less than once per week.

5.4. Instrument alignment

Pyranometers measuring global and diffuse horizontal radiation must be leveled accurately, especially if the main interest of the measurement is the determination of DNI. Accurate horizontal alignment of sensors should be checked regularly using a spirit level The levelling error should be below 0.1° (6 arc minutes). The spirit level must therefore allow to accurately detect a levelling error of 0.1°.

Any misalignment has to be avoided and needs to be rapidly detected, corrected and documented. The horizontal level of the instruments should be checked regularly (e.g. monthly) and if their pedestal or the ground around it shows signs of alteration or erosion.

Spirit levels integrated in some RSI sensors are a quick indicator of inclination, but do not provide accurate sensitivity and should not be used as the only device to level the irradiance sensor. A separate spirit level with ≤0.1° accuracy should be set on the LI-COR sensor (on the housing, covering the diffusor with the spirit level) and checked for the correct horizontal alignment in two rotational azimuthal orientations. The level is first checked in an arbitrary orientation of the spirit level, then the spirit level rotated around its azimuth axis by 180° in order to evaluate potential imperfection of the spirit levels ground plate. The ideal horizontal adjustment will not result in a perfectly centric position of the bubble within the spirit level if the spirit level itself is not perfect. For a perfect alignment and with an imperfect spirit level, the bubble will not be exactly in the center of the spirit level, but it will not change its position relative to the case of the spirit level when rotating the spirit level.

Furthermore, the shadowband has to be aligned in its rest position pointing to Geographic North in the Northern Hemisphere and to Geographic South in the Southern Hemisphere. It has to be considered that Geographic North is not Magnetic North. Depending on the region, deviation of Geographic North to Magnetic North can reach around 30º. The shadowband alignment to North is not a very strict requirement, but should not exceed an angle of approximately 5º.

5.5. Datalogger clock accuracy

Apart from its general function of assigning a correct timestamp to each measurement record and integrating the correct selection of sample values for each timestamp (e.g. minute averages), the datalogger's internal clock is used for calculating the sun position, and hence is vital for correct DNI calculation. Even high quality datalogger clocks may drift by up to 1 second per month. Hence, neglecting to verify the datalogger clock accuracy for several months may already lead to significant deviations. Drifting datalogger clocks can be avoided by automated synchronization

through the data collection software, by automated synchronization to an internet time server, or with an integrated or connected GPS device.

The time zone setting must also be considered during planning of the measurement campaign, and all data acquisition, analysis and reporting adjusted accordingly. Using daylight saving time should be avoided since it leads to 1-hour time stamp jumps which need to be dealt with correctly, and in the event of setting the clock back by one hour, to the loss of one hour's worth of data on most datalogger systems which simply overwrite the affected time stamps.

If a clock deviation is detected, it is important to document its extent, direction and exact time of correction. If 1-second resolution data has been stored and collected, it may be possible to correct higher temporal aggregation data by re-calculating minute or hourly values. If 1-second resolution data has not been stored, this correction is nearly impossible, but at least the data can be utilized with awareness of the issue.

5.6. Data collection and analysis

An automatic data collection capability using a suitable communications system is recommended for high-quality, reliable measurements. The data should be screened regularly (e.g. week-daily) for evaluation of data quality and measurement failures. Regular screening enables fast detection of issues and avoids long periods with data loss or defective data.

For the post processing of the measurement data an adequate quality assessment, flagging and gap filling method should be applied to generate high quality and as far as possible gapless data sets. Continuous time series without gaps are required since the most applications, like models for plant performance simulations, require gap less data sets. Appropriate automatic procedures for quality assessment and gap filling are topics in IEA PVPS Task 16 and several publications ([Long2002], [Maxwell1993], [Wilcox2011], [Journee2011], [Espinar2011], [Geuder2015], [Forstinger2021a], [Blanc2023]). In addition to automatic procedures, further visual inspection by an expert is required as automatic procedures cannot detect all erroneous data and some correct data points might be flagged erroneously. Visual inspection of the data enables the detection of problems that may be overlooked by automated programs. Specialized data acquisition and quality management software exists (e.g. [Geuder2015], [Maxwell1993]). A procedure for analysis and adjustment for soiling effects should be included in the analysis software and explained to the local personnel in charge for the regular inspections and sensor cleaning.

Optional redundant measurements can be of great help for data quality assessment and can increase data reliability and availability. In addition to an RSI, a second RSI, or merely a thermal pyranometer or an additional LI-COR pyranometer for simple additional GHI measurements or satellite derived data and nearby other measurement stations can be used in such a case. If correction functions are applied to the data directly on the datalogger, saving also the raw data before these corrections can be of interest.

5.7. Documentation of measurements and maintenance

Required documentation (see also Best Practices Handbook section 3.6):

- Written maintenance procedure for station keeper with exact formulation of tasks to be done (in local language, with pictograms or station photographs illustrating the sensors and required tasks)
- Date and time of sensor cleaning by station
- Special occurrences with date, time and description (sensor or power outages, …)
- Adjustment procedure/method for irradiance data (flagging of all data manipulations)
- Applied data processing and quality control procedures
- Changes of the instrumentation or the surroundings of the station require updates of the documentation listed in the previous section.
- Gaps and eventually gap filling method with corresponding information (flagging techniques)
- Observed datalogger clock time shifts, time and date of correction

Electronic documentation is recommended

- Electronic documentation whenever possible
- Equip measurement station with a button to be pressed at sensor cleaning for leaving an electronic entry in the data set

6. Adjustments for RSI irradiance measurements

RSIs with continuous rotation need a detector with a fast response time (much less than 1 second—e.g., approximately 10 µs). Therefore, thermopile sensors cannot be used, and hence the above described RSIs use the Si photodiode-based pyranometers LI-200SA or LI-200R. These pyranometers have systematic spectral, cosine, and temperature errors and corrections should be applied to improve the accuracy. These correction functions are also called adjustment functions. Several sets of correction functions that reduce systematic errors in RSI readings have been developed. The systematic effects are described in the next section followed by a description of some of the most important sets of correction functions.

6.1. Spectral, cosine response and other systematic errors of the LI-200 pyranometer

The photoelectric effect is quantitatively described by Equation 1, Equation 2 and Equation 3.

$$\phi = h \cdot f_0 \qquad \textbf{Equation 1}$$

$$hf = \phi + E_{k,\max} \qquad \textbf{Equation 2}$$

$$E_{k,\max} = \frac{1}{2} \cdot m_e \cdot v_m^2 \qquad \textbf{Equation 3}$$

Φ: Minimum energy required to remove a delocalized electron from the band
$E_{k,max}$: Maximum kinetic energy of ejected electrons
h: Planck's constant
f: Frequency of the incident photon
f_0: Threshold frequency for the photoelectric effect to occur
m: Rest mass of the ejected electron
v_m: Velocity of the ejected electron

The equations imply that if the photon's energy is less than the minimum energy Φ, no electron will be emitted since an emitted electron cannot have negative kinetic energy. If the photon has more energy than Φ this energy will partly be converted to kinetic energy and not to electric energy. The spectral response refers to the part of the photon’s energy that can be converted to electric energy. It is typically given relative to its maximum. The response of photoelectric pyranometers is not the same for all wavelengths within the solar spectrum as it is seen in Figure 3, which illustrates the spectral response of the LI-200SA pyranometer. The sensor only responds to wavelengths between 0.4 and 1.2 µm. The diffusor filters out photons with wavelengths below 0.4 µm. Its spectral response within this interval is not uniform. The response to blue light is noticeably lower than for red light and colorinfrared radiation. This inhomogeneous spectral response causes a spectral error of the broadband irradiance measurement.

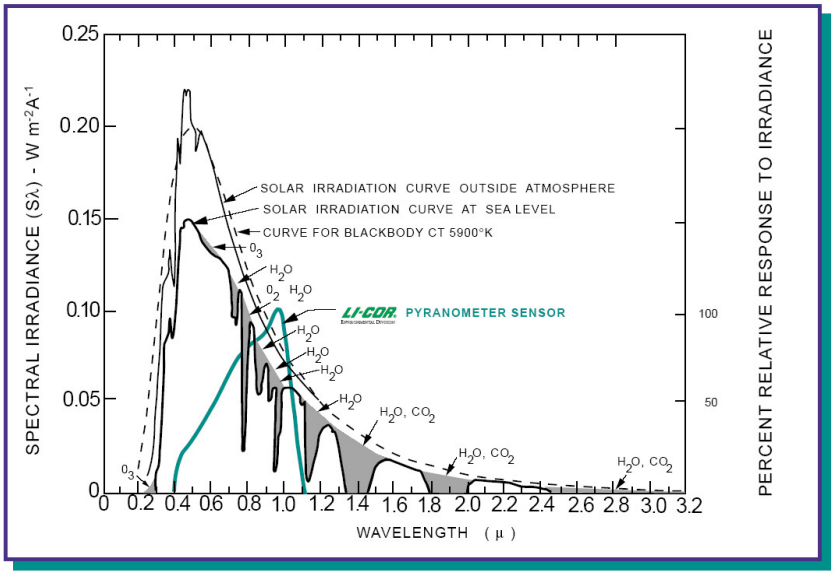

Figure 3: LI-200 pyranometer spectral response along with the energy distribution in the solar spectrum, [Biggs2000]

Although the LI-200 Pyranometer is called a cosine corrected sensor, it has a typical cosine bias of up to 5 % for wavelengths below an 80° angle of incidence [Biggs2000], as shown in Figure 4. The shape of the diffusor disk causes the responsivity to decrease dramatically at angles greater than 82.5°. Totally diffuse radiation introduces a cosine error of around 2.5 %. For a clear sky and a sun elevation of 30°, the error cosine is approximately 2 %. The LI-200 azimuth error is less than ±1 % at 45°.

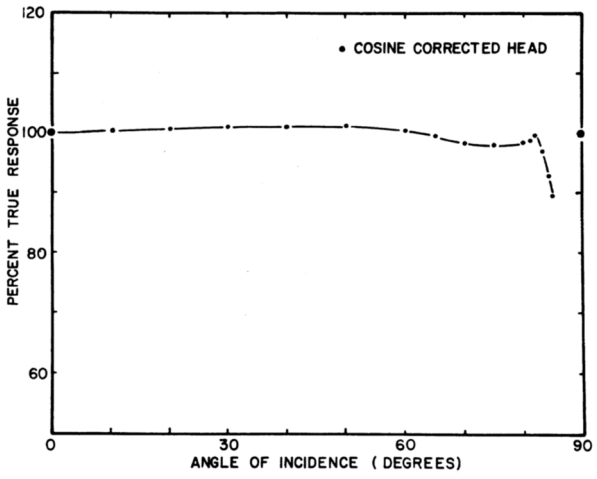

Figure 4: Cosine response of LI-COR terrestrial type sensors, [Biggs2000]

The LI-COR sensor has a temperature dependence in the order of 0.08 %/K. The spectral response changes with the temperature, allowing less energetic photons to contribute to the photocurrent at higher temperatures and leading to this increase of sensitivity with temperature.

Although temperature and cosine responses of photodiode pyranometers have been well documented, the accuracy to which these systematic errors can be corrected is influenced by the atmospheric conditions, the solar position and the spectral response as the spectral distribution changes.

Several research groups have developed adjustment functions that reduce the systematic errors of RSIs. Whereas temperature adjustments are widely coincident in all versions, the methods for the spectral effects vary between the publications. Due to the correlation between the solar spectrum and the solar elevation, spectral adjustments and incidence angle adjustments are often connected.

Different approaches for the spectral adjustments are listed in the following. [Alados1995] uses tabular factors for different sky clearness and skylight brightness parameters and a functional correction depending on the incidence angle. [King1997] proposes functional corrections in dependence on airmass and the angle of incidence derived for global irradiance. This approach was further developed by [Vignola2006] including also diffuse and subsequently direct beam irradiance. Independently, a method was developed by the German Aerospace Center (DLR) using functional adjustment including a particular spectral parameter composed from the irradiance components of global, diffuse and direct irradiance in 2003 and improved in 2008 [Geuder2008]. Additional adjustments in dependence on airmass and incidence angle were used. Further more physical corrections are under development ([Vignola2019], [Forstinger2020]). Another interesting development includes the combination of an RSI with a co-located thermopile pyranometer [Lezaca2018]. The most relevant adjustments are presented in this chapter.

6.2. Adjustments by King, Myers, Vignola, Augustyn

King, et al., Augustyn et al. and Vignola developed and published different versions of adjustment functions for the Si-pyranometer LICOR LI-200SA [LICOR2005]. The adjustments depend on the sensor temperature, the solar zenith angle, the air mass (AM), DHI and GHI. In the presented version of the adjustment functions the GHI is adjusted in the first step as described in section 6.2.1. The adjusted GHI is then used for the calculation of the DHI adjustment (section 6.2.2). Finally, the adjusted values for DHI and GHI are used together with the zenith angle to determine the DNI.

6.2.1. GHI Correction by King and Augustyn

The presented correction for GHI consists of work published in a series of publications. The first part of the corrections were published in [King1997]. One year later, King et al. published an update of their work in which some of the coefficients of the correction functions are given with more digits [King1998]. Later, Augustyn added one further correction factor based on these publications in [Augustyn2002]. In 2004, an update of this work was presented, in which the coefficients were given with more digits [Augustyn2004]. This document presents one complete set of GHI correction functions that is selected using the different available publications.

The selected correction makes use of four parameters

- F_α: the temperature parameter
- F_A; the spectral response parameter
- F_B: the cosine response parameter and
- F_C: the cat ear parameter

and is formulated as

$$GHI_{corr} = GHI_{raw} \cdot \frac{F_\alpha}{F_A F_B F_C}$$ ***Equation 4***

[Augustyn2004] with the uncorrected (raw) GHI (GHI_{raw}) and the corrected GHI (GHI_{corr}).

The four parameters the adjustment are determined with the following formulas:

- F_α (temperature correction by [King1997]; with the coefficient of temperature dependence $\alpha = 8.2 \cdot 10^{-4}$ and the reference temperature T_{ref} = 25°C; T_{LICOR} also in °C)

$$F_\alpha = 1 - \alpha \cdot (T_{LICOR} - T_{ref})$$ ***Equation 5***

- F_A (spectral response correction by [King1998]; with airmass *AM*)

$$F_A = 2.631 \cdot 10^{-4} \cdot AM^3 - 6.319 \cdot 10^{-3} \cdot AM^2 + 5.401 \cdot 10^{-2} \cdot AM + 0.932$$

Equation 6

- F_B (cosine response correction factor by David King [King1998]; solar zenith angle SZA in degree):

$$F_B = -4.504 \cdot 10^{-7} \cdot SZA^3 + 1.357 \cdot 10^{-5} \cdot SZA^2 + 6.074 \cdot 10^{-4} \cdot SZA + 1$$

Equation 7

- F_C (cat ear adjustment by Augustyn [Augustyn2004] (solar zenith angle *SZA* in degree)):

$$F_C = \begin{cases} 10.164664 - 0.24242 \cdot SZA + 1.603 \cdot 10^{-3} \cdot SZA^2 & ; \quad 75° < SZA < 81° \\ -58.03442 + 1.457577 \cdot SZA - 8.99 \cdot 10^{-3} \cdot SZA^2 & ; \quad 81° \le SZA < 83.2° \\ 1 & ; \quad 0° \le SZA \le 75° \vee SZA \ge 83.2° \end{cases}$$

Equation 8

In absence of direct temperature data from the pyranometer, T_{LICOR} can be estimated by following equation of unknown source.

Estimated pyranometer temperature in °C:

$$T_{LICOR} = T_{air} + (-4.883 \cdot 10^{-6} \cdot GHI_{raw}^2 + 0.00953 \cdot GHI_{raw} - 0.5)$$

Equation 9

Figure 5 illustrates the estimation of the temperature dependence and its coefficient α by linear regression.

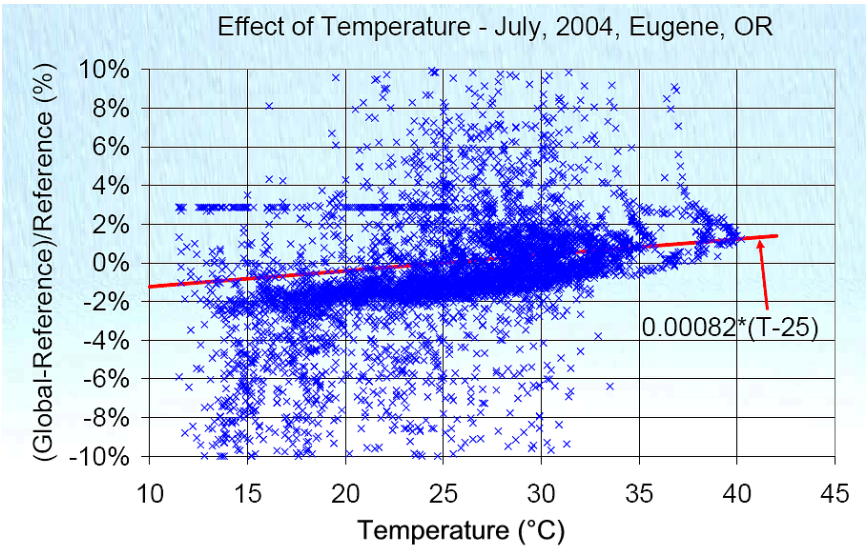

Figure 5: Temperature dependence on LI-COR 200SA pyranometer, Courtesy of F. Vignola.

The above stated functions are used e.g. at DLR for the calibration of RSIs. It should be mentioned that other versions of the correction exist due to the deviations between the different published versions of the corrections. A summary of these deviations is given in the following. [Vignola2006] presented a new version of the global corrections, with an updated spectral correction (F_A) that closely matches the results for F_A obtained using the formula from [King1998], but fits the results better for high *AM* according to [Vignola2006]. The expressions for F_A and F_B in [Vignola2006] are the same as the ones given above from [King1998]. For F_C and zenith angles between 75° and 81° one coefficient in [Vignola2006] deviates from [Augustyn2004] and unrealistic results are obtained with the value from [Vignola2006]. For the other range of zenith angles the coefficient in front of *SZA* deviates by less than 0.2 % from the corresponding coefficient from [Augustyn2004]. This small deviation cannot be explained or excluded by comparison to reference irradiance data, but it can be assumed that the deviation from the values given in [Augustyn2002] and [Augustyn2004] is by error.

In [King1997b] the coefficient in front of SZA in Equation ***7*** for F_B is given as $6.074 \cdot 10^{-5}$ instead of $6.074 \cdot 10^{-4}$. As $6.074 \cdot 10^{-4}$ is used in all other publications it can be assumed that $6.074 \cdot 10^{-4}$ is the correct coefficient.

The Cat Ear Correction was implemented in order to deal with the increase of deviations at zenith angles above 75° which peak at about 81° as shown in Figure 6 and Figure 7.

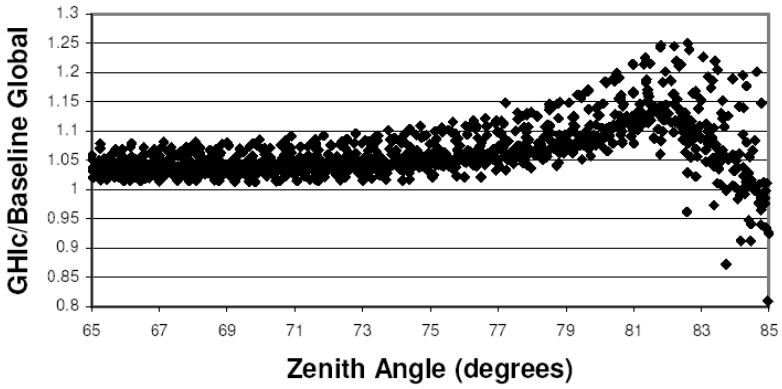

Figure 6: NREL GHI_{corr}/baseline GHI from 65-85° Zenith Angle: The Cat Ear error [Augustyn2002]

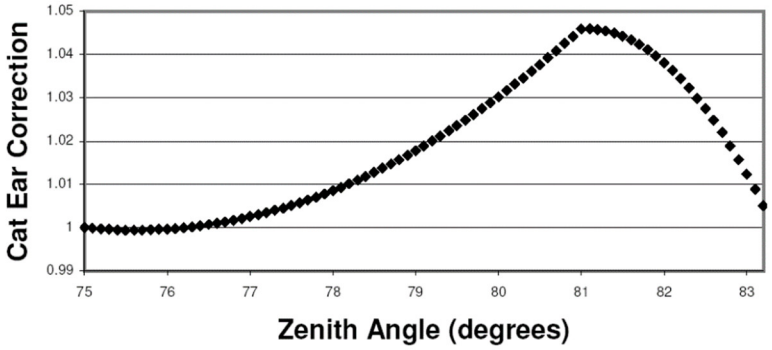

Figure 7: Cat Ear Correction [Augustyn2002]

6.2.2. DHI correction by Vignola et al. (2006)

The applied version of Vignola's diffuse correction makes use of the corrected GHI and the uncorrected DHI. For $GHI_{corr} \leq 865.2$ W/m² the correction is performed as

$$DHI_{corr} = DHI_{raw} + GHI_{corr} \cdot (-9.1 \cdot 10^{-11} \cdot GHI_{corr}^{3} + 2.3978 \cdot 10^{-7} \cdot GHI_{corr}^{2} \ldots \ldots - 2.31329234 \cdot 10^{-4} \cdot GHI_{corr} + 0.11067578794)$$

Equation 10

For higher GHI_{corr} the correction is expressed as

$$DHI_{corr} = DHI_{raw} + GHI_{corr} \cdot (0.0359 - 5.54 \cdot 10^{-6} \cdot GHI_{corr})$$

Equation 11

The diffuse correction has been published in different versions in [Vignola1999], [Augustyn2002], [Augustyn2002] and [Vignola2006]. The first work by Vignola presented a correction for GHI > 100 W/m² that was later only used for high GHI levels (> 865.2 W/m²). The following two publications ([Augustyn2002] and [Augustyn2004]) used another formula developed by Vignola in the meanwhile for GHIs below this value. Furthermore, they applied the correction using uncorrected GHI as variable. [Vignola2006] works with the corrected GHI and states that the corrections were developed for use with high quality GHI measurements and that they still work with corrected GHI values from RSIs. Thus, the presented diffuse correction works

with the corrected GHI signal. In [Vignola2006] a small deviation in one of the coefficients for the diffuse correction with GHI ≤ 865.2 W/m² appears. The change is less than 0.001 % and the value stated in [Augustyn2002] and [Augustyn2004] is used above.

With increasing GHI the diffuse error of the unrectified DHI value increases significantly in comparison to the corrected DHI (Figure 8).

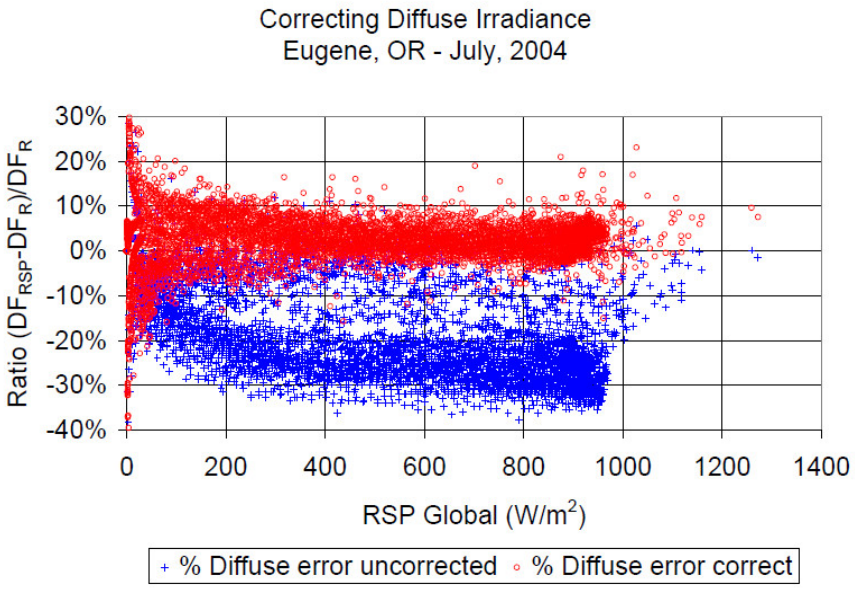

Figure 8: Comparison of DHI_{raw} (here DF_{RSP}) and DHI_{corr} (here DF_R) against GHI_{raw} (here RSP Global) [Vignola2006]

6.3. Corrections by Batlles et al.

Previously a different approach to DHI correction was published by Batlles and Alados-Arboledas [Batlles1995]. It included the use of tabular factors for different sky clearness and sky brightness parameters and a functional correction depending on the incidence angle. Sky clearness and sky brightness are considered functions of cloud conditions and the presence of aerosols respectively. The first is derived from DNI_{raw} and DHI_{raw}, while the latter is determined by DHI_{raw}, the solar zenith angle and the extraterrestrial solar irradiance. The correction factor is then calculated with linear regressions for different ranges of sky brightness, which is the second most significant parameter in this model after the solar zenith angle.

While the [Batlles1995] method focusses on sky conditions, the later developed DHI correction by [Vignola2006] as presented in section 6.2.2 produced higher accuracy by using a corrected GHI value on the basis of temperature, spectral influences and solar zenith angle instead of sky conditions and solar zenith angle.

6.4. Corrections by DLR

For the derivation of correctional functions, the quotient of the reference irradiance to the corresponding RSI signal was calculated for every data point (available time

resolutions were 1 and 10 minutes, respectively). This quotient represents the (running) correction factor CF_r to correct the measured RSI value in order to receive the reference irradiance. Data sets of 23 different RSI were used within the evaluation, taken within a period of an entire year. As the raw RSI irradiance was determined just with the original LI-COR calibration factor, each data set was corrected for this rough calibration with a draft constant correction previous to the derivation of the functional coherences.

6.4.1. Correction of the temperature dependence

Measurements on RSI temperature dependence were performed with two different methods:

- Measuring the sensor signal under real sky conditions (around solar noon) and temperature inside the sensor head while it was warming up from 0°C to around 40°C.
- Measuring the sensor signal and temperature under artificial illumination (a stabilized lamp) when the sensor was cooling down from 60°C to 5°C.

In both cases the signals of two reference photodiodes at constant temperature were used to eliminate minor variations of irradiation during the measurement. Both methods yielded nearly the same factor of 0.0007/K for the temperature dependence of the LI-COR sensor head in agreement with the value given by [King1997]. Figure 9 shows this dependence of the correction factor on temperature as gained from the measurements under real sky conditions. The factor for correcting the temperature influence is calculated along:

$$C_{temp} = (1 - 0.0007 \cdot (T_{LICOR} - 25\,°C)) \qquad \textbf{Equation 12}$$

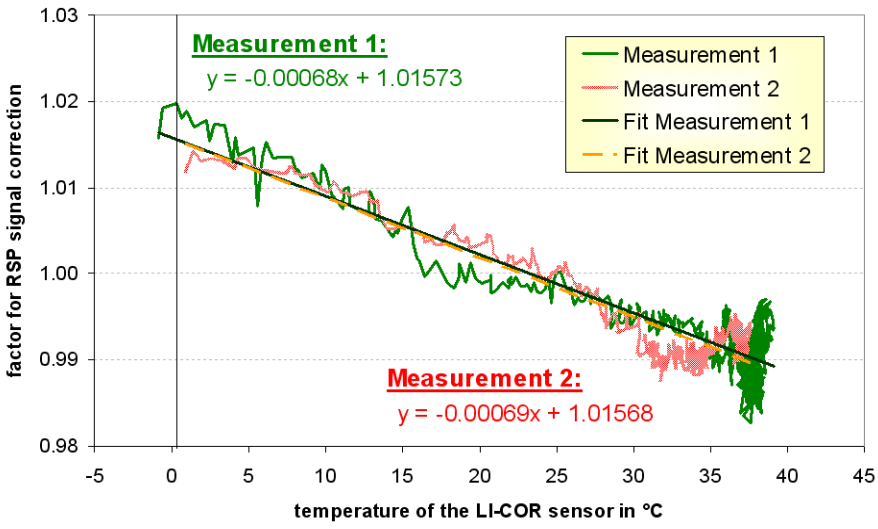

Figure 9: Correction factor for the LI-COR sensor response as a function of temperature.

6.4.2. Spectral influence on diffuse irradiation

To obtain a suitable parameter to correct the spectral dependence, various parameters including e.g. sky clearness parameter and skylight brightness parameter as well as further numerous combinations of accessible measured values were analyzed. A parameter with a comparably narrow spread of the CF_r around the main curve was found (see Figure 10). This spectral parameter, Π_{spec}, is calculated along:

$$\Pi_{spec} = DNI \cdot GHI / DHI^2 \quad . \qquad \textbf{Equation 13}$$

CF_r is described as a function with a linear and an exponential term with Π_{spec} as variable and its coefficients as linear functions of the ambient temperature.

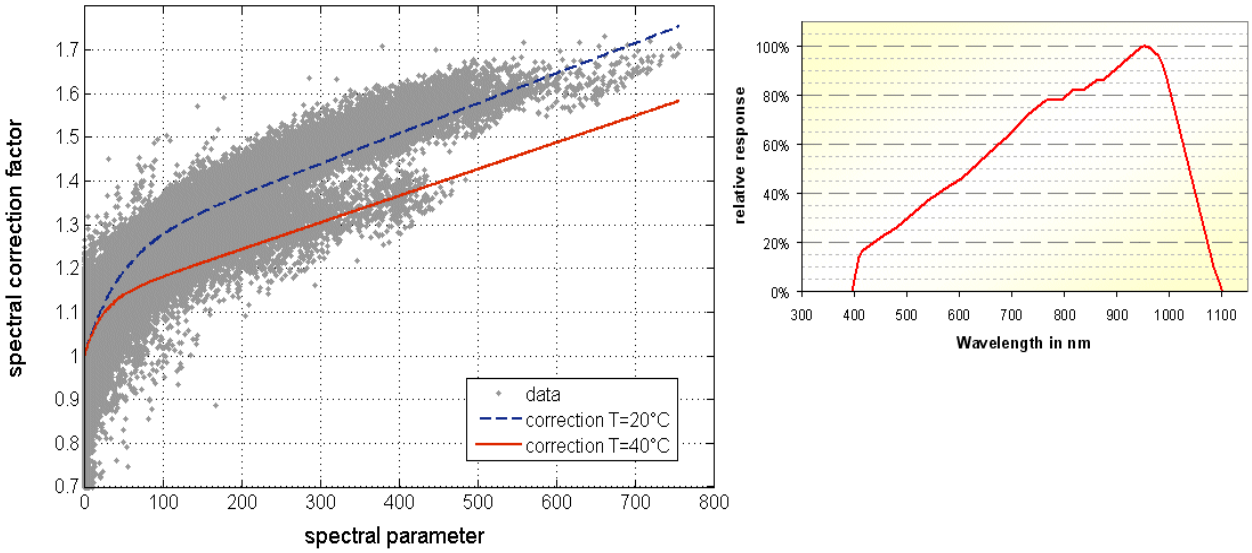

Figure 10: Correction Factor of diffuse irradiance as a function of the spectral parameter Π_{spec} = DNI·GHI / DHI² and the ambient temperature (left) and spectral response curve of the LI-200SA sensor (right).

The impact of the spectral correction can clearly be seen comparing original and spectrally corrected DHI in the right graph of Figure 11: the uncorrected raw DHI has a clear peak up to values of 1.8 at small Air Mass Factor (AMF), which disappears with the spectral correction.

6.4.3. Correction of Air Mass dependence

The Air Mass Factor (AMF) is used for another correction automatically including the altitude of the location. AMF is calculated along [Young1994], pressure-corrected with measured values or – in absence of measurements – calculated via the international height formula, including ambient air temperature. The true solar zenith angle (without refraction), necessary here for calculation of AMF, is determined along [Michalsky1988].

The spectrally corrected CF_r of DHI in the right chart of Figure 11 are located within a clearly delimited band at small AMF values (high solar elevations) within values of 0.8 and 1.2, smoothly decreasing with rising AMF (lower solar angles) and with a

rising spread of the values. The mean curve could be well approximated with a second order polynomial in AMF and was fitted to the spectrally corrected DHI.

The running correction factors of the GHI RSI data also show dependence on the air mass factor. However, to see the correct correlation, previously the influence of direct beam response at low sun elevations (described in section 6.4.4) has to be eliminated in analogy to the spectral factor at DHI. Without the direct-beam influence, a similar smooth dependence of global CF_r on the AMF emerges (see left graph in Figure 11) and is corrected with a second order polynomial in AMF with different coefficients.

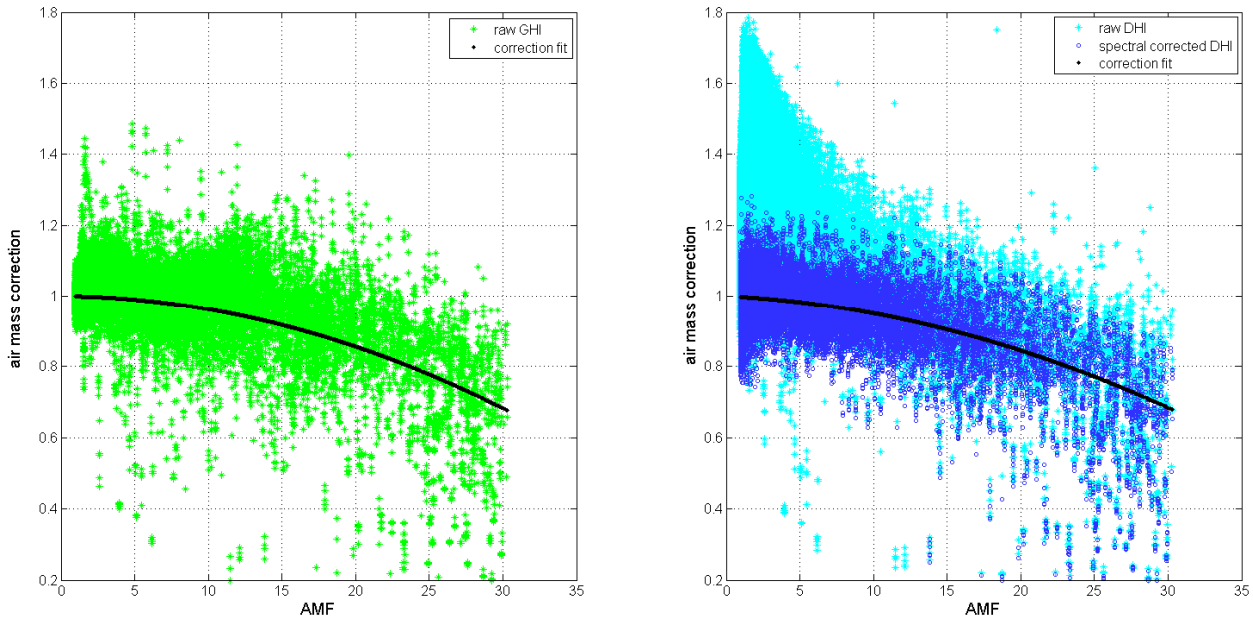

Figure 11: Correction of the RSI response in dependence on the pressure-corrected air mass factor AMF for global horizontal irradiance (left) and diffuse horizontal irradiance (right) with and without spectral correction.

6.4.4. Correction of the directional response of the LI-COR sensor in dependence on the incidence angle

Vice versa eliminating the influence of air mass from the global CF_r values, a characteristic dependence on the incidence angle turns up. The response is affected in particular at incidence angles beyond 75 degrees. High incidence angles here correspond to low solar elevations as in our case the sensor is always mounted horizontally. Unfortunately, the overall accuracy is poor at high incidence angles in combination with the non-ideal cosine correction and maybe non-ideal leveling as well as small irradiances. Therefore, a mean curve of the AMF-corrected global data was determined from the point cloud of widely spread values to visualize the dependence. The mean curve of the data is plotted in Figure 12 together with the fit of the correction function. The exact form of the mean curve is varying slightly among the various data sets supposedly due to minor variations in mounting and assembly of the LI-COR sensor as well as maybe also due to seasonal/spectral effects. However, its characteristic form is similar among all data sets and is known as the "cat-ear" effect [Augustyn2004].

The correction function represents the sum of an exponential and a combined sinusoidal and exponential term with the solar elevation as variable for solar elevations over 3 degrees and a steadily connected linear function for lower solar height angles.

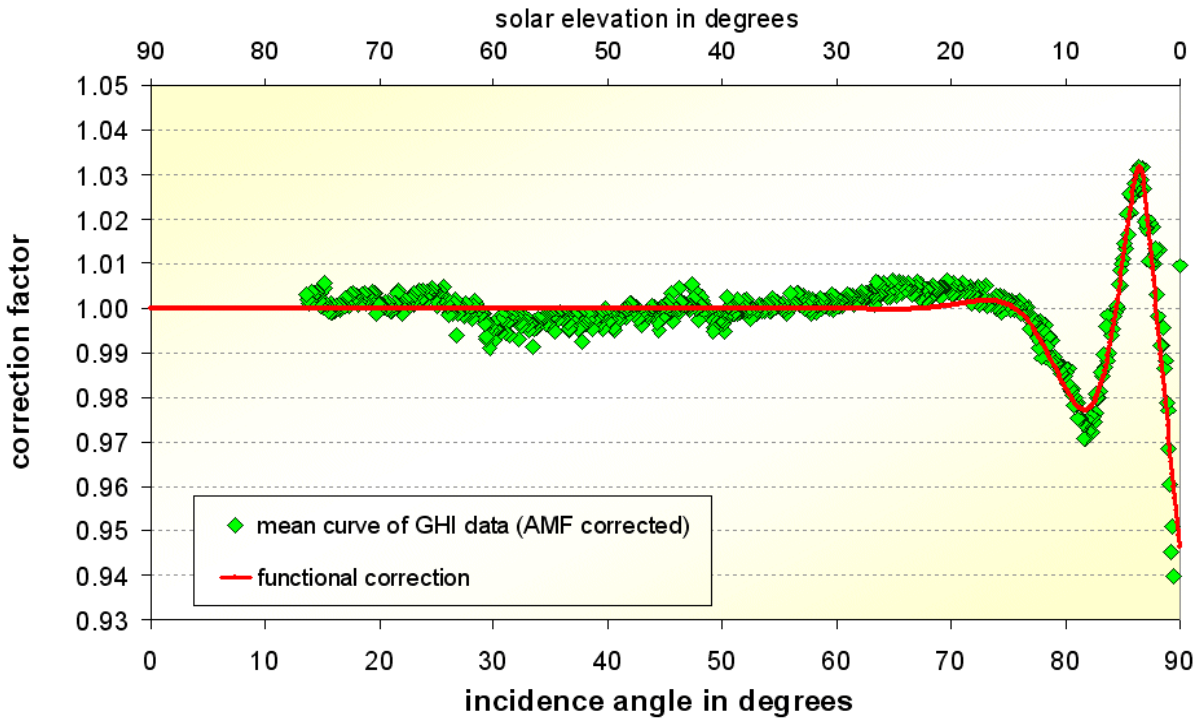

Figure 12: Mean curve of (AMF-corrected) CF_r of global horizontal irradiance in dependence on the angle of incidence

6.4.5. Correction of remaining errors: intensity and constant factor

After the above corrections, the DHI is still marginally overestimated for intensities over 350 W/m², which is partly corrected with an additional cubic function on DHI. The remaining deviation of DNI is partly corrected with a linear function of DNI.

With finally all former presented corrections applied, new constant correction factors CF were determined for each RSI separately for global and diffuse irradiation. The correction factors and functions refer to the original calibration factor from LI-COR Inc. From the 23 analyzed RSIs, an average constant *CF* of 1.023 for global irradiation and 1.32 for diffuse irradiation with corresponding standard deviations of 0.9 % and 1.4 % was derived, respectively. The variability of the *CF* values is illustrated in Figure 13 separately for GHI and DHI. The y axis represents the relative deviation of each *CF* to the denoted average values.

Figure 13: Variability of the constant Correction Factors CF for global and diffuse irradiance, plotted as relative deviation to the average CF of the analyzed Reichert GmbH Rotating Shadowband Pyranometer. The slide-in chart at the top shows the variability between the global and diffuse CF.

For single sensors maximal deviations of 3 % from the mean value were found for diffuse and below 2 % for global irradiance. However, in addition to the variability of the constant factors among different RSIs, the quotient from the global and diffuse correction factor varies within 2.5 % (on average: 1.1 %). This variability is not corresponding to seasonal variations nor could other obvious reasons be stated. Intrinsic differences of the individual pyranometers, for example the spectral sensitivity might explain the variation of the quotients. Finally, two separate correction factors are determined at the calibration for global and diffuse irradiation as explained in section 7.

6.5. Corrections by CSP Services

For the development of enhanced corrections, 39 different RSIs at different sites and climate zones have been examined by CSP Services, based on data over a range of 2 years. Finally, the following correlations were elaborated.

6.5.1. Correction of Diffuse Horizontal Irradiance

A similar correction as in [Geuder2008] over the spectral parameter $PI = DNI \bullet GHI / DHI^2$ is applied. Figure 14 shows this dependence with the ratio of reference to raw RSI DHI as an ascending blue colored band plotted over *PI*.

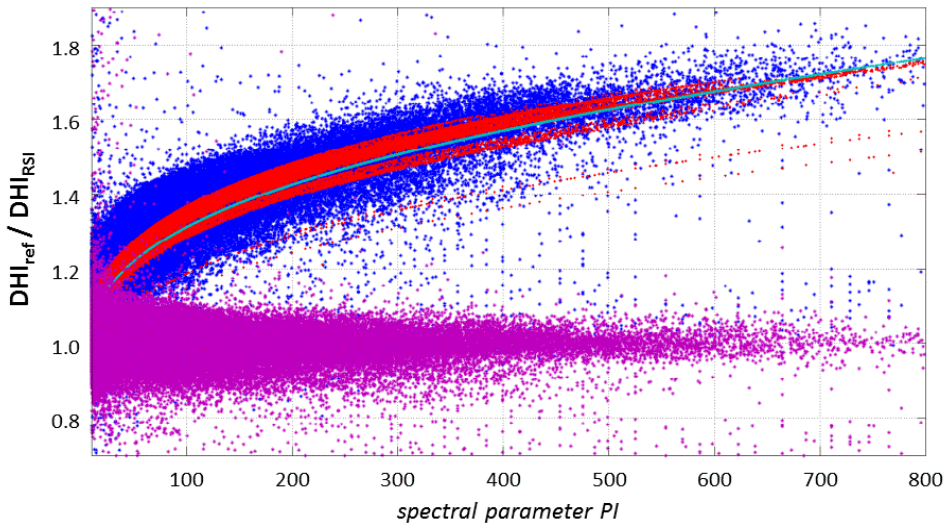

Figure 14: Ratio of DHI values of reference to RSI data before correction (blue) and with applied correction (purple) in dependence on the spectral parameter. The turquoise line shows the spectral correction, the red data points include additional varying air mass and/or altitudes.

A further error in the diffuse irradiance response in the order of <5 % was attributed to the variation of the air mass in dependence on solar elevation and site altitude. Hence, additional terms depending on air mass and site altitude are used by the CSP Services correction functions. The full DHI correction (including spectral dependence, air mass and altitude correction) is also depicted in Figure 14. The turquoise line represents the spectral correction function *f(PI)* for a particular airmass and altitude. Its course changes with varying airmass and different site altitudes. This is plotted with the red data points for an air mass range of 1 to 38 and site altitudes between 0 and 2200 m. The purple band finally refers to the ratio mentioned above, but for corrected RSI data and is spread around a value of 1, meaning coincident DHI values.

6.5.2. Correction of Global Horizontal Irradiance

GHI is composed by two components: the direct solar beam and the hemispherical diffuse irradiance originating from the sky. With the impacts on the diffuse component treated yet, the influences presented in the following act merely on the direct component and are therefore applied only on the portion of the Horizontal Direct Beam Irradiance: *BHI = GHI - DHI*.

An important contribution to the RSI's error on the direct component results from angular effects at low solar elevations. Measurements of the response of the LI-COR pyranometer in dependence on the incidence angle of the solar beam yield a characteristic deviation in the order of 10 % (see Figure 15). This effect was yet referred by further authors as the so-called "cat-ear" effect. An angular correction below an apparent sun height of 20° as shown by the green line in Figure 15 is applied to the BHI portion of GHI. Furthermore, the influences of the varying spectrum of the direct solar beam with changing air mass are respected with a similar corresponding correction like at the diffuse component.

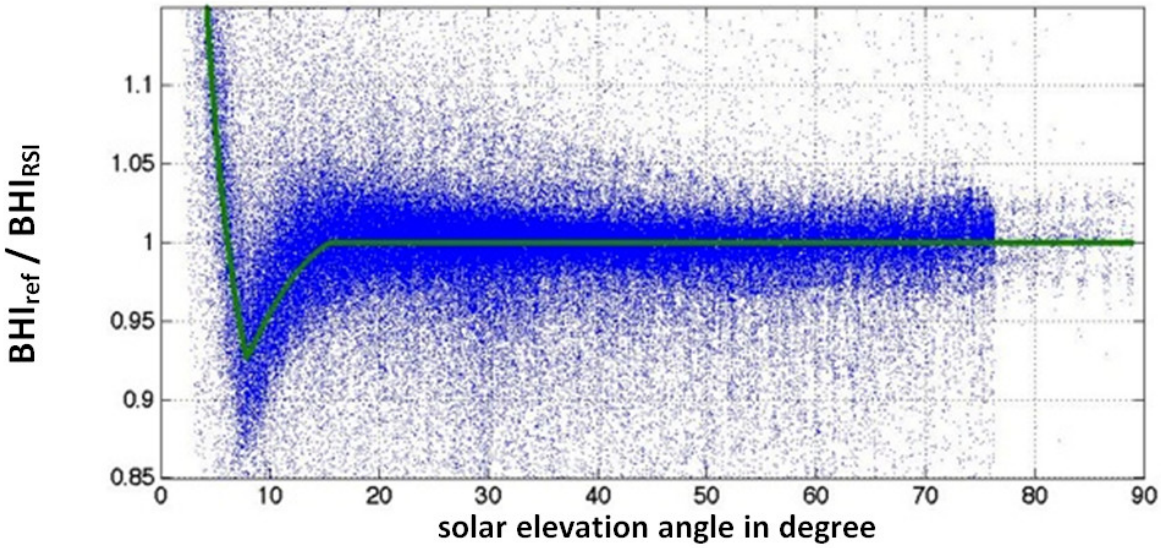

Figure 15: BHI ratio of reference to RSI measurements (blue data points) and corresponding correction function (green line) in dependence on the solar elevation angle, showing the "cat-ear" peak at low solar elevations

6.5.3. Altitude correction for GHI and DHI

After applying the mentioned corrections on the measured global and diffuse irradiances, a dependence on the altitude of the measurement site above mean sea level has been detected for some sensors analyzed and calibrated at some selected sites around Almería with different altitudes. The dependence on the site altitude is presented in Figure 16. This observation has been confirmed with devices which have been installed in other regions and countries aside high-precision instruments at altitudes deviating from the 500 m altitude of CIEMAT's PSA. Therefore, an additional correction for site altitude is used for GHI and DHI with 500 m of PSA as mean reference altitude.

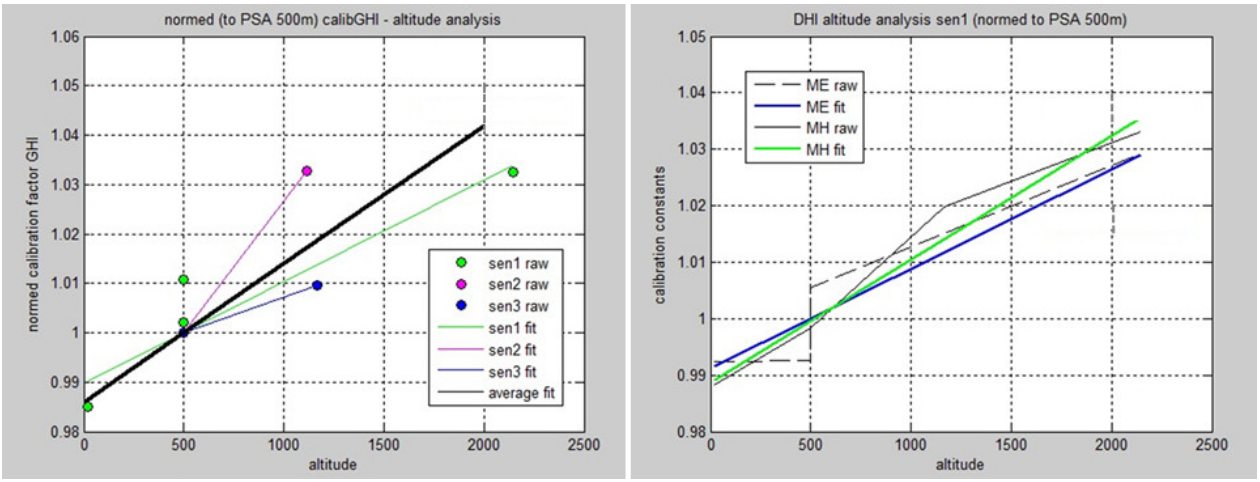

Figure 16: Dependence of the Calibration Factor CF on the altitude above mean sea level for GHI (left) and for DHI (right)

6.5.4. Calculation and correction of Direct Normal Irradiance

The DNI is finally calculated from GHI, DHI and the apparent solar elevation [Michalsky1988]. A final minor linear intensity correction is also applied to DNI.

6.6. Correction algorithm based on simultaneous thermal GHI measurements

Another option for the correction of the RSI raw data makes use of a co-located thermopile pyranometer that measures GHI [Lezaca2018]. The GHI correction from equation 4 is modified by replacing the terms for the air mass and zenith angle factors by regression functions that minimize the GHI deviations of the RSI from the thermopile pyranometer for the last days or weeks. These functions are adapted daily to represent the more recent sky conditions better. The DHI correction from section 6.2.2, and the DHI correction approaches from sections 6.4 and 6.5 have been tested in combination with this dynamic GHI correction. The method simplifies the calibration process as the RSI can be calibrated dynamically on site. The complications related to the DHI correction and spectral errors of DHI and DNI remain as the GHI thermopile pyranometer does not provide detailed information on the contributions of DHI and DNI to the measured GHI. An additional RSI specific calibration for DHI or DNI is not used for this method.

7. Calibration of RSIs

In order to provide accurate irradiance measurements, a thorough calibration of the RSIs is indispensable. Besides, the stability of the sensor sensitivity needs to be controlled within the measurement period. In the following a summary of the calibration of RSIs is presented. Further details can be found in [Jessen2017]. Note that the correction method using a co-located thermopile pyranometer is only discussed in section 6.6 due to the combination of the correction and calibration for this method.

7.1. Calibration Methods

The calibration of an RSI is crucial for the system performance and more than the calibration of the pyranometer alone. A pre-calibration of the commonly used pyranometer in RSIs is carried out by the manufacturer against an Eppley Precision Spectral Pyranometer for 3 to 4 days under daylight conditions. Further calibration efforts are usually performed for the application in RSIs.

Due to the rather narrow and inhomogeneous spectral response of the photodiodes and the combined measurement of DHI and GHI, extra care has to be taken when using the existing standards for the calibration of radiometers for RSI calibration. The calibration methods described in ISO 9846 [ISO9846 1993] and ISO 9847 [ISO9847 2023] for pyranometers and in ISO 9059 [ISO9059 1990] for pyrheliometers are

based on simultaneous solar irradiance measurements with test and reference instruments recorded with selected instrumentation. The annex of ISO 9847 for pyranometers refers to calibrations with artificial light sources.

Calibration of RSI instruments involves calibration for DNI, DHI and GHI. Due to the spectral response of the instrument it can be problematic to calibrate based on only a few series of measurements and under the special conditions defined in and ISO 9059. The calibration only holds for the calibration conditions and calibration under conditions that are very different from those that are present during the later measurements can lead to errors. This is possible for thermal sensors due to their homogenous spectral response covering the bulk of the solar spectrum. Therefore, some calibration methods intent to include a wide variety of meteorological conditions in the calibration period. The accuracy of the measurements generally improves when the conditions during the calibration represent the conditions at the site where the RSI is operated. In addition to the cloud cover, the influences of aerosols, water vapor, temperature and site altitude have to be considered. Calibrations with artificial radiation sources usually lack the variety of irradiation conditions; therefore, field calibrations under natural irradiation conditions are preferred.

RSI calibrations are performed for example at NREL in Golden, Colorado or by DLR on CIEMAT's Plataforma Solar de Almería (PSA) in Spain. In all of the presented cases, RSIs are operated outdoors parallel to thermopile radiometers (see Figure 17 and Figure 18). The duration of this calibration is between several hours and several months. Data quality is analyzed and compared to the reference irradiances.

Other methods are possible, too, although they are not described and evaluated here. One not further documented, but promising approach to calibrate a photodiode pyranometer is to establish a reference photodiode pyranometer of the same model and use the reference pyranometer to calibrate the photodiode based pyranometer under study. The temperature response, cosine response, and spectral response of the reference pyranometer will be similar enough to the pyranometer being calibrated, that a decent calibration number can be obtained. This is especially true if the responsivity is normalized to a reference solar zenith angle, e.g. 45°.

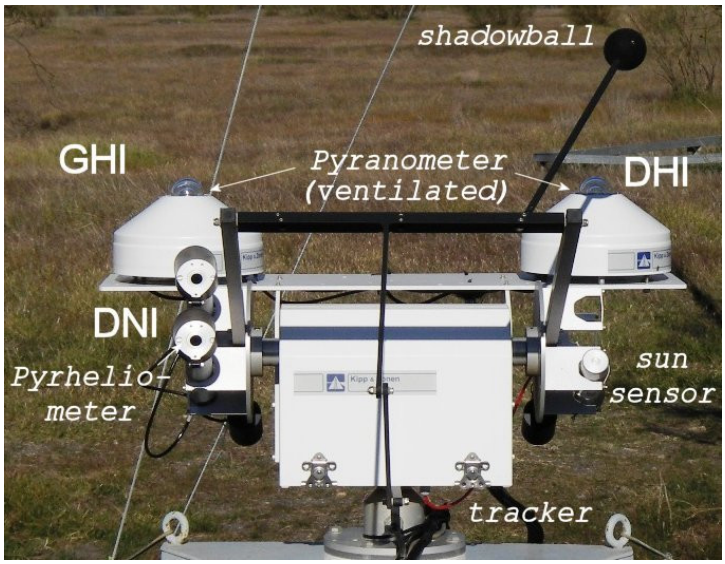

Figure 17: Thermopile radiometers (left picture) at CIEMAT's Plataforma Solar de Almería.

Figure 18: RSI calibration mount of DLR at CIEMAT's Plataforma Solar de Almería.

7.1.1. Method 1

The constant calibration factor and the diffuse correction are determined by comparing the precise direct normal and diffuse horizontal irradiance to corresponding RSI irradiance data as determined with the LI-COR calibration constant and including correction functions from [Geuder2008]. The RMS (root mean square) deviation of the 10-minute means for DHI is minimized by variation of the thereby determined diffuse correction. Then the RMS deviation for the DNI is minimized using the constant calibration factor. Irradiation data from the RSI and the DLR station is logged as 60 second averages during the entire calibration process. For calibration, only the relevant operation range of solar thermal power plants is considered with DNI >

300 W/m², GHI > 10 W/m², DHI > 10 W/m² and at sun height angles > 5°. Outliers with deviations of more than 25 % are not included. In order to contain sufficient variation of sky conditions, the measurement interval covers at least two months. Two correction factors are defined (one for DHI one for GHI).

7.1.2. Method 2

Another approach for RSI calibration involves the correction functions presented by [Vignola2006]. The other aspects are very similar to the ones described in method 1. The subset of data used for the calculation of the calibration factors is slightly different (DNI>250 W/m², outliers defined as deviation of more than 15 %). Three correction factors are defined here. After applying the correction functions, the thus calculated GHI, DNI and DHI are multiplied with a constant respectively. First, the RMS deviation of the 10-minute means for GHI is minimized by variation of the thereby determined GHI calibration constant. Then the RMS deviation for the DHI and finally that of the DNI is minimized using the corresponding constants.

7.1.3. Method 3

A further method suggested by [Kern2010] uses only GHI data for the calculation of a calibration factor. This allows the calibration of the LICOR sensors without a shading device. Exclusively measurements collected for solar zenith angles between 56.8° and 58.8° are used, collected in intervals with low temporal variation of GHI and low deviation of DNI to its theoretical clear sky value according to [Bird1984].

7.2. Effect of the duration of outdoor calibrations

The effect of the duration of the outdoor calibration has been investigated in [Geuder2014] and [Jessen2016]. The RSIs were operated in parallel to a reference meteorological station at CIEMAT's Plataforma Solar de Almería as presented for calibration method 1 for many months. The data sets were used for multiple calibrations of the RSIs using different durations of the calibration period from 1 day to 5 or 6 months, respectively. The various calibration results were grouped according to the length of the calibration interval and compared to the calibration based on the complete data set. Separate calibration constants were determined for DNI, GHI and DHI.

The result of the analysis from [Geuder2014] is shown in Figure 19. In Figure 19 the deviation of the daily, weekly and monthly average of the ratio of the reference DNI and the corrected RSI derived DNI from the corresponding long-term average ratio derived from the complete data set is shown. No significant drift can be seen for DNI. For the corresponding ratios for DHI the variation is more pronounced. The data show that the calibration result and the required duration of the calibration depend on the sky conditions. Even if an RSI is used at the same site at which it is calibrated short calibration durations of only a few days may lead to significant errors. Longer calibration durations reduce the observed deviations.

In [Jessen2016] also seasonal effects were investigated. Seasonal changes of sky conditions were found to cause noticeable fluctuations of calibration results. Calibrations during certain periods (e.g. November to January and April to May) showed a higher likelihood of deviations from the long-term average calibration result. While for some periods a calibration duration of only two weeks already led to a good reproduction of the long-term calibration, for some periods of the year 2 or even 3 months calibration durations were required to reproduce the long-term results within 2%. Calibrations with method 1 using only data from November reached better agreement with the long-term result than calibrations using November and December.

The findings of the existing studies on calibration duration stress the importance of the calibration conditions for the accuracy of the measurements. The calibration conditions should be as representative as possible for the conditions during the planned measurement campaign. This holds also if the calibration is done at the same site at which the RSI is used later.

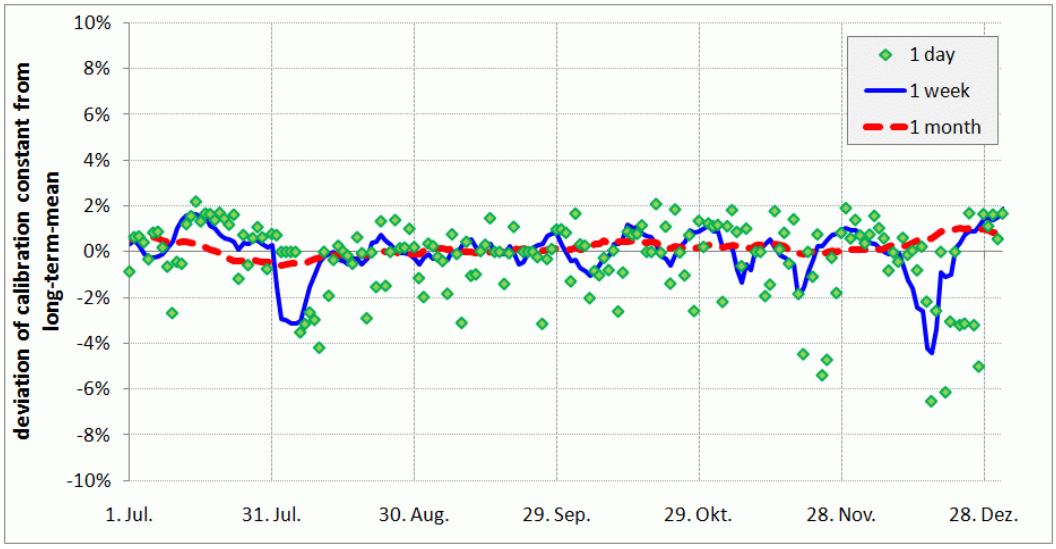

Figure 19: Variation of the average ratio DNI_{corr}/DNI_{ref} for daily, weekly or monthly calibration (as running average) over a period of 18 months

8. RSI uncertainty

The accuracy of RSIs has been investigated in several works based on comparisons with thermopile pyrheliometers and pyranometers as well as using analytical uncertainty calculations. [Forstinger2021b] provides an overview of those studies and describes an analytical approach for the uncertainty calculation. Benchmarks of RSIs and other simple radiometers measuring diffuse and/or direct irradiance have been presented in [Vuilleumier2017] and [Blum2023] and comparably low deviations have been found.

The accuracy of RSIs is approximately 2.5%–4% for GHI and 3% to 9% for DNI, if proper calibration and correction functions are used (standard uncertainty, 1 sigma, 10 min resolution [Forstinger2021b]). The lower uncertainty limit is only reached if the calibration conditions correspond well to the measurement conditions and for deployment at sunny sites. The above described correction functions and the condition-specific calibration reduce the uncertainties compared to uncorrected measurements that are based only on the manufacturer calibration of the photodiode pyranometer. For comparison, in well maintained field measurement campaigns with solar trackers and pyrheliometers for DNI and pyranometers for GHI and DHI standard uncertainties of about 1.5% for DNI and 2% for GHI can be reached [Sengupta2021]. However, the initially higher uncertainty of RSIs compared to ISO 9060 Class-A pyrheliometers and pyranometers for optimal maintenance conditions is often compensated by some unique advantages of RSIs. Their simplicity/robustness, low soiling susceptibility [Geuder2006; Pape2009; Maxwell1999], low power demand, and comparatively lower cost (instrumentation and O&M) provide significant advantages compared to thermopile sensors and solar trackers, especially at remote sites. This can also be quantified in terms of uncertainty when considering the soiling effect, tracking errors and data gaps in the site-specific uncertainty analysis.

9. Conclusion and Outlook

RSIs have proven to be appropriate instruments for diligent solar resource assessments for large-scale solar plant projects.

As for all meteorological sensors best practices must be followed to allow for utmost data quality. Well defined procedures must be followed for

- the selection of location for measurement station,
- installation, operation and maintenance of measurement station, including the case of remote sites,
- the documentation and quality control of the measurements,
- and the correction of systematic biases & instrument calibration (procedure and frequency)

as presented in this document. Due to their lower maintenance requirements, lower soiling susceptibility, lower power demand, and comparatively lower cost, RSI show significant advantages over thermopile sensors when operated under the measurement conditions of remote weather stations. The initially lower accuracy of RSIs can be notably improved with proper calibration of the sensors and corrections of the systematic deviations of its response. Uncertainties of 2.5%–4% for GHI and 3% to 9% for DNI have been found in the various studies published so far (standard uncertainty, 1 sigma, 10 min resolution).

Different RSI calibration methods exist and have been compared. Application of two or more calibration factors for the different irradiance components respectively yields noticeable higher accuracy than the application of only one calibration factor derived from GHI measurements.

The so far achieved measurement accuracy of RSIs can still be improved. The analysis of the transferability of correction and calibration between different climate zones, sites and altitudes will be continued. Further investigation of spectral and site dependent corrections is of interest.

Acknowledgements

The comments and suggestions from the reviewers and IEA SHC Task 46 and IEA PVPS Task 16 members are highly appreciated. We thank the German Federal Ministry for Economic Affairs and Energy for the financial support for the creation of the second edition of this work within the SOLREV project (FK 03EE1010) and the INS project 1268 for the financial support of the first edition. We thank Chris Kern, Gundolf Reichert and Raúl Granados for providing information concerning the RSR and RSP 4G.

Supported by:

on the basis of a decision
by the German Bundestag

References

[Alados1995] Alados-Arboledas, L., F. J. Batlles, F. J. Olmo, Solar Radiation Resource Assessment by Means of Silicon Cells, Solar Energy, Vol. 54 No. 3, 183-191 (1995).

[Augustyn2004] Augustyn, J., Geer, T., Stoffel, T., Kessler, R., Kern, E., Little, R., Vignola, F., Boyson, B., "Update of Algorithm to Correct Direct Normal Irradiance Measurements Made with a Rotating Shadow Band Pyranometer", Proc. Solar 2004, American Solar Energy Society, (2004)

[Augustyn2002] Augustyn, J., Geer, T., Stoffel, T., Kessler, R., Kern, E., Little, R., Vignola, F., "Improving the Accuracy of Low Cost Measurement of Direct Normal Solar Irradiance", Proc. Solar 2002, American Solar Energy Society, (2002)

[Batlles1995] Batlles, F. J., F. J. Olmo and L. Alandos-Arboledas: On Shadowband Correction Methods for Diffuse Irradiance Measurements, Solar Energy, Vol. 54 No. 2, 105-114 (1995)

[Blanc2023] Blanc, P., R. Amaro e Silva. Benchmarking of GHI gap-filling methods. IEA PVPS Task 16 report 03:2023. Editor: J. Remund. ISBN 978-3-07281-37-6 (2023)

[Blum2023] Blum, N., et al. A Benchmark of Simple Diffuse and Direct Irradiance Measurement Systems. Proceedings of the 35th EU PVSEC 2023 (Lisbon) (2023).

[Biggs2000] LI-COR, Inc. (William W. Biggs), "PRINCIPLES OF RADIATION MEASUREMENT", Lincoln, Nebraska, USA

[Bird1984] Bird, R.E., A simple, solar spectral model for direct-normal and diffuse horizontal irradiance. Solar Energy, 1984. **32**(4): p. 461-471.

[Espinar2011] Espinar, B.; Wald, L.; Blanc, P.; Hoyer-Klick, C.; Schroedter-Homscheidt, M. & Wanderer, T. Report on the harmonization and qualification of meteorological data Project ENDORSE, Energy Downstream Service Providing Energy Components for GMES, Grant Agreement No. 262892, 2011. Available at http://www.endorse-fp7.eu/public_deliverables

[Forstinger2020] Forstinger, Anne, Stefan Wilbert, Anton Driesse, Natalie Hanrieder, Roman Affolter, Sharad Kumar, Neeraj Goswami, Norbert Geuder, Frank Vignola, Luis Zarzalejo, and Aron Habte. 'Physically based correction of systematic errors of Rotating Shadowband Irradiometers', Meteorologische Zeitschrift. http://dx.doi.org/10.1127/metz/2019/0972

[Forstinger2021a] Forstinger, A., Wilbert, S., Jensen, A. R., Kraas, B., Peruchena, C. F., Gueymard, C. A., Ronzio, D., Yang, D., Collino, E., Martinez, J. P., Ruiz-Arias, J. A., Hanrieder, N., Blanc, P., & Saint-Drenan, Y. M. (2021). Expert quality control of solar radiation ground data sets. In Proceedings of SWC 2021: ISES Solar World Congress (pp. 1037-1048). International Solar Energy Society. https://doi.org/10.18086/swc.2021.38.02

[Forstinger2021b] Forstinger, A., Wilbert, S., Driesse, A., & Kraas, B. (2021). Uncertainty calculation method for photodiode pyranometers. Solar RRL. https://doi.org/10.1002/solr.202100468

[Geuder2006] Geuder, N., Quaschning, V., "Soling of Irradiation Sensors and Methods for Soiling Correction", Solar Energy 80, 1402-1409 (2006).

[Geuder2008] Geuder, N., B. Pulvermueller, O. Vorbrugg, Corrections for Rotating Shadowband Pyranometers for Solar Resource Assessment, Solar Energy + Applications, part of SPIE Optics + Photonics 2008, 10-14 August 2008, San Diego, USA (2008).

[Geuder2014] Geuder, N., Affolter, R., Kraas, B., and Wilbert, S.: Long-term Behavior, Accuracy and Drift of LI-200 Pyranometers as Radiation Sensors in Rotating Shadowband Irradiometers (RSI), Energy Procedia, 49, 2330–2339, doi:10.1016/j.egypro.2014.03.247, (2014)

[Geuder2015] Geuder, N., F. Wolfertstetter, S. Wilbert, D. Schueler, R. Affolter, E. Luepfert, and B. Espinar. "Screening and Flagging of Solar Irradiation and Ancillary Meteorological Data." In Proceedings of the International Conference on Concentrating Solar Power and Chemical Energy Systems, SolarPACES 2014. Beijing, China. https://doi.org/10.1016/j.egypro.2015.03.205 (2015)

[ISO9059 1990] ISO 9059:1990(E), Solar energy – Calibration of field pyrheliometers by comparison to a reference pyrheliometer, International Organization for Standardization, Case Postale 56, 1211 Genève, Switzerland (1990).

[ISO9847 2023] ISO 9847:2023(E), Solar energy – Calibration of pyranometers by comparison to a reference pyranometer, International Organization for Standardization, Case Postale 56, 1211 Genève, Switzerland (2023).

[ISO9846 1993] ISO 9846:1993, Solar energy – Calibration of a pyranometer using a, International Organization for Standardization, Case Postale 56, 1211 Genève, Switzerland (1993).

[Jessen2016] Jessen, W., Wilbert, S., Nouri, B., Geuder, N., and Fritz, H.: Calibration methods for rotating shadowband irradiometers and optimizing the calibration duration, Atmos. Meas. Tech., 9, 1601–1612, https://doi.org/10.5194/amt-9-1601-2016 (2016)

[Jessen2017] Jessen, W., Wilbert, S., Zarzalejo, Z., Ramirez, L., Valenzuela, R., Liria, J., Nouri, Hanrieder, N.: Calibration Procedures for Rotating Shadowband Irradiometers, Deliverable 11.5 SFERA 2 project report (2017)

[Journee2011] Journée, M. Bertrand, C. Quality control of solar radiation data within the RMIB solar measurements network. Solar Energy 85 (2011), 72-86.

[King1997] King, D. L., D. R. Myers, Silicon Photodiode Pyranometers: Operational Characteristics, Historical Experiences, and New Calibration Procedures, 26th IEEE Photovoltaic Specialists Conference, (1997).

[King1998] King, D. L., Boyson, W. E., Hansen, B. R., and Bower, W. I., 1998, "Improved Accuracy for Low-Cost Solar Irradiance Sensors," 2nd World Conference and Exhibition on Photovoltaic Solar Energy Conversion Proceedings; July 6–10, 1998, Vienna, Austria.

[Kern2010] Kern, E., Calibration Methods for Silicon Photodiode Pyranometers used in Rotating Shadowband Radiometers, in Proceedings of SolarPACES Conference, Perpignan (2010).

[Lezaca2018] Lezaca, J., Meyer, R., Heinemann, D.; Study of an extended correction algorithm for rotating shadowband irradiometers (RSI) based on simultaneous thermal GHI measurements. AIP Conf. Proc. 8 November 2018; 2033 (1): 190009. https://doi.org/10.1063/1.5067194 (2018).

[LICOR2001] Calibration Procedures for LI-COR Spectroradiometers, Radiation Sensors & Lamps - Application Note #109. https://licor.app.boxenterprise.net/s/e3kud5scodpe9jeerypj. (2001).

[LICOR2005] LI-COR® Biosciences, LI-COR Terrestrial Radiation Sensors – Instruction Manual, LI-COR, Inc., Lincoln, Nebraska 68504, USA (2005).

[Long2002] Long, C.N., Dutton, E.G.. Baseline Surface Radiation Network (BSRN) Global Network recommended QC tests, V2.0. http://epic.awi.de/30083/1/BSRN_recommended_QC_tests_V2.pdf, 2002 (last accessed 2014-09-25).

[Maxwell1993] Maxwell, E., Wilcox, S. and Rymes, M. Users Manual for SERI QC Software. Assessing the Quality of Solar radiation Data. Technical report NREL TP-463-5608 DE93018210. 1993. Available at http://www.nrel.gov/docs/legosti/old/5608.pdf (last accessed 2014-09-26).

[Maxwell1999] Maxwell, E., S. Wilcox, C. Cornwall, S. Alawaji, B. Marion, M. bin Mahfoodh, and A. Al-Amoudi. 1999. “Progress Report for Annex II--Assessment of Solar Radiation Resources in Saudi Arabia 1993-1997.” National Renewable Energy Lab.(NREL), Golden, CO (United States).

[Michalsky1988] Michalsky, J. J., “The Astronomical Almanac’s Algorithm for Approximate Solar Position (1950-2050)”, Solar Energy Vol. 40, No. 3, 227-235 (1988).

[Pape2009] Pape, B., Battles, J., Geuder, N., Zurita, R., Adan, F., Pulvermueller, B., Soiling Impact and Correction Formulas in Solar Measurements for CSP Projects, Proceedings of SolarPACES Conference, Berlin (2009).

[Sengupta2021] Sengupta, M., Habte, A., Wilbert, S., Gueymard, C., and Remund, J. (editors). Best practices handbook for the collection and use of solar resource data for solar energy applications. No. NREL/TP-5D00-77635. National Renewable Energy Lab.(NREL), Golden, CO (United States) / IEA PVPS Task 16 report. ISBN 978-3-907281-19-22021.

[Vignola1999] Vignola, F., “Solar Cell Based Pyranometers: Evaluation of Diffuse Responsivity”, Proceedings of the 1999 Annual Conference American Solar Energy Society, June 1999, (1999).

[Vignola2006] Vignola, F. Removing Systematic Errors from Rotating Shadowband Pyranometer Data, Solar 2006, American Solar Energy Society, 7th – 13th of July 2006, Denver, Colorado, USA, (2006).

[Vignola2019] Vignola, F., Peterson, J., Mavromatakis, F., Wilbert, S., Forstinger, A., Dooraghi, M., and Sengupta, M.. 2019. 'Removing biases from rotating shadowband radiometers', AIP Conference Proceedings, 2126: 190017.

[Vuilleumier2017] Vuilleumier, L., Félix, C., Vignola, F., Blanc, P., Badosa, J., Kazantzidis, A., and Calpini, B.. 2017. “Performance Evaluation of Radiation Sensors for the Solar Energy Sector.” Meteorologische Zeitschrift. (2017).

[Wilbert2018] Wilbert, S., Röger, M., Csambor, J., Breitbach, M., Klinger, F., Nouri, B., Hanrieder, N., Wolfertstetter, F., Schüler, D., Shaswattam, S. and Goswami, N., 2018, November. Sunshape measurements with conventional rotating shadowband irradiometers. In AIP Conference Proceedings (Vol. 2033, No. 1, p. 190016). AIP Publishing LLC.

[Wilcox2011] Wilcox, S. Cormack, P. Implementing Best Practices for Data Quality Assessment of the National Renewable Energy Laboratory’s Solar Resource and Meteorological Assessment Project. SOLAR 2011, Raleigh, North Carolina, May 16-21, 2011.

[WMO2018] WMO, 2018, "Guide to Meteorological Instruments and Methods of Observation, WMO-No. 8, Seventh edition 2018 update."

[Young1994] Young, A. T., “Air Mass and Refraction”, Applied Optics Vol. 33 No. 6, (1994).